Theoretical and Applied Fracture Mechanics 114 (2021) 103024

Contents lists available at ScienceDirect

Theoretical and Applied Fracture Mechanics

journal homepage: www.elsevier.com/locate/tafmec

Mechanisms of fatigue crack growth in Ti-6Al-4V alloy subjected to single overloads

D.M. Neto, M.F. Borges *, F.V. Antunes, J. Jesus

Univ Coimbra, Centre for Mechanical Engineering, Materials and Processes (CEMMPRE), Department of Mechanical Engineering, Portugal

ARTICLE INFO

Keywords:
Fatigue crack growth
Overload
Crack closure
Residual stresses
Finite element method

ABSTRACT

The relative importance of crack closure and residual stresses on fatigue crack growth (FCG), which is controversial, is studied here. FCG is predicted numerically in CT specimens of Ti-6Al-4V alloy submitted to single overloads, assuming that crack tip plastic strain is the driving force. The numerical procedure, which includes the effects of crack tip blunting, material hardening, crack closure and partial crack closure, was found to be very robust and to give correct trends. The high strength material studied showed relatively small overload affected zones (<0.5 mm), which is even more pronounced under plane strain conditions. The comparison of numerical results with and without contact of crack flanks showed that crack closure is responsible for the effect of overloads on FCG rate behaviour, while the effect of residual stresses is not relevant for the material studied. The transient behaviour obtained after an overload is unattainable without considering the contact of the crack flanks.

1. Introduction

Real components and structures are typically submitted to complex loading patterns. Therefore, different standard load patterns have been proposed like TWIST and FALSTAFF sequences for transport and fighter aircraft, respectively, or CARLOS for automotive applications [1]. The TWIST load spectrum [2], for example, has an average of a thousand small gust cycles per flight with a major cycle associated with the ground-air-ground sequence and a few overloads associated with more severe atmospheric turbulence. Design against fatigue based on damage tolerance approach requires the knowledge of fatigue crack growth (FCG) rate. However, there is a great complexity associated with these standard load patterns and with real patterns, and it is important to start studying simpler patterns for a progressive understanding of the underlying mechanisms. The study of overloads is a good starting point for the understanding of variable amplitude loading and has been widely studied. The overloads are also interesting because they can be intentionally used to extend the fatigue life of components [3] and to delineate the shape of the crack front [4].

The variation of FCG rate after an overload is well-known. There is a sudden peak of *da/dN* followed by a decrease to a minimum value, after which there is a progressive increase towards the constant amplitude *da/dN* [4–7]. The minimum FCG rate occurs after some propagation, which is called delayed retardation. Different mechanisms have been proposed to explain post-overload variations, namely, crack closure [8,9], residual stresses [10], crack tip blunting [11], strain hardening [12,13] and crack branching [14]. However, although the huge number of studies already developed, there is not a consensus about the relative importance of these mechanisms, and its dependence to loading and material.

Plasticity Induced Crack closure (PICC) is generally considered the primary cause of post-overload retardation [5]. The overload enlarges the monotonic plastic zone and blunts the crack tip, eliminating totally or partially the crack closure phenomenon. The crack growth through this plastically deformed material generates a new plastic wake, which gives higher values of PICC, comparatively to the previous constant amplitude values [15]. Ishihara *et al.* [16] and Shin and Hsu [17] demonstrated that crack closure is able to explain the transient crack growth behaviour following overloads. Lu *et al.* [7] found a good correlation between the variations of *da/dN* and PICC. However, a mismatch was found between the crack lengths corresponding to the minimum value of *da/dN* and the maximum value of PICC. To check to dominance of crack closure effect, *da/dN* is usually plotted versus the effective stress intensity factor range, ΔK_{eff} [5,7].

The plastic deformation at the crack tip produces a region of compressive residual stresses, which is amplified by the overload. These residual stresses may be predicted numerically or measured

* Corresponding author.
E-mail address: fernando.ventura@dem.uc.pt (M.F. Borges).

https://doi.org/10.1016/j.tafmec.2021.103024
Received 30 January 2021; Received in revised form 21 April 2021; Accepted 19 May 2021
Available online 21 May 2021

Nomenclature

a	Crack length
a_{OL}	Crack length where the overload was applied
C, Y_0 and n	Isotropic hardening parameters
CTOD	Crack Tip Opening Displacement
CA	Constant Amplitude
CT	Compact Tension (specimen)
C_X, X_{Sat}	Kinematic hardening parameters
da/dN	Fatigue crack growth rate
DIC	Digital Image Correlation
F	Remote load
F_{max}	Maximum baseline load
F_{min}	Minimum baseline load
F_{open}	Crack opening load
F_{OL}	Peak load
FCG	Fatigue Crack Growth
K	Stress intensity factor
MT	Middle Tension (specimen)
N_{D1}	Number of delay cycles
N_{D2}	Number of cycles to achieve the steady state
N_{OL}	Load cycle where the overload was applied
OL	Overload
OLR	Overload ratio ($=\Delta F_{OL}/\Delta F_{BL}$)
PICC	Plasticity Induced Crack Closure
R	Stress ratio
SEM	Scanning Electron Microscopy
U^*	Crack closure level (in percentage)
Δa	Total crack propagation
Δa_{min}	Crack increment measured from the overload to the minimum da/dN
Δa_{OL}	Crack increment from the position where the overload was applied
ΔF_{BL}	Load range of the baseline cycle ($=F_{max}-F_{min}$)
ΔF_{OL}	Load range of the overload ($=F_{OL}-F_{min}$)
ΔN_{OL}	Number of load cycles applied after the overload
ΔK	Stress intensity factor range ($=K_{max}-K_{min}$)
ΔK_{BL}	Baseline cyclic stress intensity factor range
ΔK_{eff}	Effective stress intensity factor range ($=K_{max}-K_{open}$)
$\Delta\varepsilon^p$	Total plastic strain

experimentally using X-ray diffraction [18]. Salvati *el at.* [18] studied the relative importance of residual stresses ahead of crack tip and crack closure on crack retardation following an overload. Crack closure was inhibited considering a high stress ratio R = 0.7. They concluded that although the residual stress effect is present at all values of R, it disappears rapidly with crack growth, whilst crack closure is dominant at low values of R and has a longer influence. Lu *et al.* [7] proposed a modified Wheeler model based on residual stresses and PICC effects. The research conducted by Sunder *et al.* [19] suggested that both residual stress effect and crack closure effect had an influence on the overload retardation. Chen *et al.* [20] concluded that compressive residual stress played a dominant role while crack closure was secondary in overload-induced retardation even in the case of lower baseline R of 0.11 under plane stress state. Simpson *et al.* [21] using high energy synchrotron concluded that residual stresses are dominant at R = 0.1, but not at R = 0.4, when crack growth beyond overload was small and while the crack remained within the overload plastic zone ($\Delta a_{OL}/r_{p,OL} < 0.6$, being Δa_{OL} the crack growth after the overload and $r_{p,OL}$ the size of overload plastic zone). Lopez-Crespo *et al.* [22] concluded that the causes of crack growth retardation could be attributed to compressive residual stresses ahead of the crack tip by measuring the fatigue crack tip strain fields following a 100% overload under plane strain conditions with an in-situ synchrotron X-ray diffraction.

The crack tip blunting was observed numerically [15,23] and experimentally using Scanning Electron Microscopy, SEM, [24]. Crack tip blunting causes rounding of the crack tip, i.e., the sharp crack is replaced by a notch. This reduces stress concentration and therefore FCG rate. Crack tip blunting also separates crack flanks, reducing or eliminating instantaneously crack closure, as already mentioned. However, it cannot account for the existence of delayed retardation [25]. The application of overloads has also been shown to produce crack tip branching and deflexion at the moment of application [20]. Suresh [26] suggests that a bifurcated crack tip profile is subjected to a lower ΔK_{eff} than a straight crack of the same projected length subjected to an identical value of far-field stress intensity factor, ΔK. Meggiolaro *et al.* [27] studied post-overload retardation effects on SAE 4340 steel submitted to single overload ratios, OLR = 100%. They argued that the crack growth retardation is associated with crack branching. However, Aguilar Espinosa *et al.* [25] argued that the bifurcation observed by Meggiolaro *et al.* cannot fully account for the retardation, because it is significantly smaller than the crack extension affected by the overload. The irregular crack path caused by crack branching enhances the roughness-induced closure. Material hardening associated with overload is also a possible mechanism. Strain hardening reduces the ductility of material with a consequent reduction in the resistance of crack propagation which is supposed to increase da/dN [28]. On the other hand, material hardening reduces crack tip plastic deformation with a consequent reduction of FCG rate. In other words, material hardening has opposite effects on static and cyclic damage mechanisms.

The main objective here is to improve the understanding of FCG in Compact Tension (CT) specimens submitted to single overloads, with a particular emphasis on the underlying mechanisms. A numerical approach was followed based on the cumulative plastic strain at the crack tip, assuming that FCG is driven by crack tip plasticity. The effects of PICC, partial closure, residual stresses ahead of crack tip, crack tip blunting and material hardening are included in a natural way, since they affect the crack tip plastic strain, which makes this approach very interesting. Additionally, the contact of crack flanks can be deactivated, in order to remove its effect on da/dN, and to check the relative importance of residual stresses and crack closure. This approach, although very interesting, has not been exploited by other authors.

2. Numerical model

The numerical simulations were performed with the in-house finite element code DD3IMP, which was originally developed for the numerical simulation of sheet metal forming processes [29]. The mechanical model considers large elastoplastic strains and assumes that the elastic strains are negligibly small with respect to unity. The elastic behaviour is assumed to be isotropic, while the plastic behaviour is described by an associated flow rule and the evolution of yield surface is defined by the work hardening law.

2.1. Finite element model

In this study, CT specimen according to ASTM E647 [30] standard is subjected to mode I cyclic loading. The detailed configuration of the CT specimen is illustrated in Fig. 1. Due to symmetry in mode I loading, only half model is considered in the numerical simulation. The meshing of the CT specimen was generated using 8-node hexahedral finite elements, adopting a selective reduced integration technique [31] to avoid volumetric locking. Since the crack tip is a zone with severe gradients of stress and strain, the mesh was refined at this region, as shown in Fig. 2a. The finite element mesh must be sufficiently refined to enable the

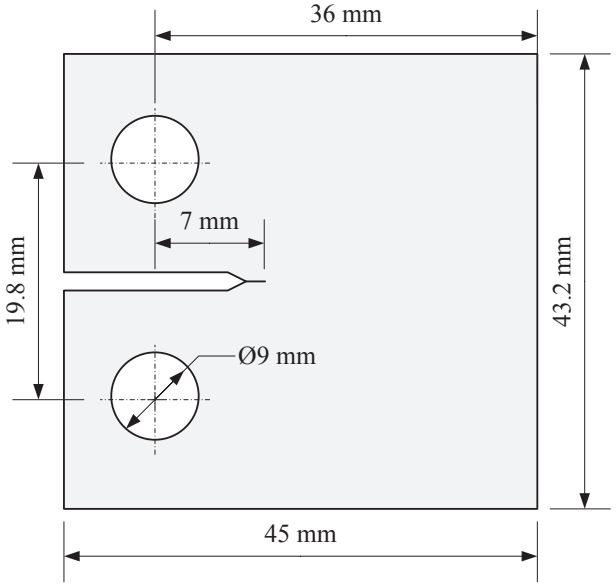

Fig. 1. Dimensions of the CT specimen (thickness of 6 mm) used in the experimental tests.

simulation of the plastic deformation phenomena occurring at the crack tip, namely, the formation of the forward and reversed plastic zones [32]. Accordingly, a relatively fine mesh with an element size of 8 μm was used in the region ahead of the crack tip in the crack growth direction. The hole in the numerical model was created with square geometry (identical area) to simplify the mesh generation procedure. In order to reduce the computational effort of the numerical solution, only a single layer of elements was used in the thickness direction while the remote zone of the specimen is defined by a coarse mesh.

Plane strain conditions were considered by constraining the out of plane displacements in both faces of the specimen, as illustrated in Fig. 2b. Additionally, plane stress conditions were also adopted by allowing the out of plane displacements in a single face of the specimen, as shown in Fig. 2c. Nevertheless, the specimen thickness was significantly reduced in the numerical model to achieve plane stress conditions using solid finite elements. The cyclic loading was applied in the top area of the hole (upper central point), simulating the contact between the pin and the specimen hole. Besides, the displacement in x direction was constraint in this point to suppress the rigid body motion. The cyclic loading was applied using a triangle waveform with constant frequency. Since the specimen used in the numerical model presents 0.1 mm of thickness, the minimum and maximum applied loads were $F_{min} = 2.2$ N and $F_{max} = 44.05$ N, respectively. These values were obtained from the experimental work developed in the same material, using CT specimens with a thickness of 6 mm [33]. Besides, in this study the overload ratio (OLR) was defined as [10]:

$$OLR = \frac{F_{OL} - F_{min}}{F_{max} - F_{min}} = \frac{\Delta F_{OL}}{\Delta F_{BL}} \tag{1}$$

where F_{max}, F_{min}, and F_{OL} are the maximum baseline, minimum baseline and peak loads, respectively.

The crack closure is the contact of crack flanks during a portion of the load cycle, which delays the intrinsic mechanisms responsible for crack growth. Therefore, it is considered in the modelling of fatigue crack growth. Indeed, crack closure seems to be able to explain the transient crack growth behaviour following overloads [15] and the influence of mean stress in both regimes I and II of crack propagation. The contact of the crack flanks is modelled considering a rigid plane (frictionless conditions) aligned with the crack symmetry plane. A master–slave algorithm is adopted, using the augmented Lagrangian method for the resolution of the mechanical frictionless contact problem [34].

2.2. Constitutive material model

The numerical analysis of the fatigue crack growth was performed for the Ti-6Al-4V alloy produced by selective laser melting. The specimens were post-processed by hot isostatic pressing to reduce the porosity and improve the fatigue life. The application of fatigue cyclic load generates a cyclic plasticity phenomenon ahead of crack tip. Thus, an accurate description of the hardening law is essential to model the plastic behaviour. Hence, the Bauschinger effect was considered in the finite element model, using a mixed hardening constitutive model comprising both isotropic and kinematic hardening on plasticity.

The isotropic hardening behaviour is described by the Swift law, where the flow stress is given by:

$$Y = C(\varepsilon_0 + \bar{\varepsilon}^p)^n \;\; with \;\; \varepsilon_0 = \left(\frac{Y_0}{C}\right)^{1/n}, \tag{2}$$

where $\bar{\varepsilon}^p$ denotes the equivalent plastic strain, while C, Y_0 and n are the

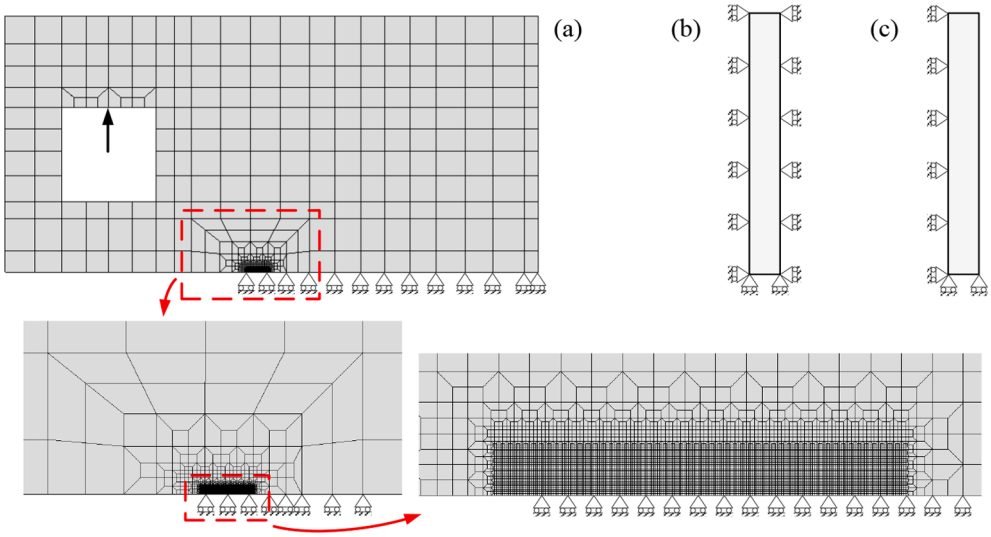

Fig. 2. Model of the CT specimen: (a) Discretization with details of the finite element mesh; (b) Plane strain boundary conditions; (c) Plane stress boundary conditions.

isotropic hardening parameters. The kinematic hardening behaviour is described by the Armstrong-Frederick model [35], which can be written as:

$$\dot{X} = C_X\left(X_{Sat}\frac{\sigma' - X}{\bar{\sigma}} - X\right)\dot{\bar{\varepsilon}}^p, \quad (3)$$

where σ' is the deviatoric Cauchy stress tensor, $\boldsymbol{X}$ is the back-stress tensor and $\bar{\sigma}$ is the equivalent stress. C_X and X_{Sat} are the kinematic hardening parameters. The calibration of the isotropic and kinematic hardening parameters for this material was carried out by Ferreira *et al.* [36] using the stress–strain curves of low cycle fatigue tests. The obtained hardening parameters are listed in Table 1.

2.3. Crack propagation

In this study, the fatigue crack propagation was simulated by successive debonding of nodes. A straight crack front was modelled, where the crack propagated uniformly over the thickness by releasing both current crack front nodes. During numerical simulation, the crack can be incremented at maximum load or at minimum load. Although the crack extension is a progressive process occurring during the entire load cycle, several authors [37] found that the load at which the crack increment occurs does not significantly influence the numerical results. Therefore, in this study the crack propagation occurs at minimum load, avoiding convergence problems caused by propagating the crack at maximum load. Considering the refined mesh around the crack tip, each crack increment corresponds to one finite element (8 μm). Thus, the FCG rate is defined by the ratio between this crack increment and the total number of load cycles required to debond the nodes.

The total number of load cycles required to debond the crack front nodes is predicted according to the proposed fatigue crack growth criterion. In this study, FCG is assumed to be controlled by plastic deformation in the zone around the crack tip [38]. Thus, the presented fatigue crack growth criterion, called Total Plastic Strain (TPS) crack growth criterion, is based on total plastic strain value, $\Delta\varepsilon^p$, at the crack tip. Debonding of nodes occurs when the total plastic strain exceeds a critical plastic strain value. Critical values of accumulated plastic strain of 1.533 and 1.215 were defined in a previous work for plane stress and plane strain states, respectively, comparing experimental *da/dN* values with numerical predictions [36]. Note that the critical value of accumulated plastic strain is supposed to be a material property, independent of loading parameters or stress state. The thickness of the specimens in the experimental work was 6 mm [36], which does not give pure plane stress or plane strain state. This is the only reason why two critical values are proposed. The equivalent plastic strain is usually computed at the integration points of each finite element. Nevertheless, the crack propagation occurs by debonding of nodes. Therefore, the equivalent plastic strain is also evaluated at the nodes of the finite element mesh (mean value of the neighbouring integration points). Indeed, the study carried out by Brito *et al.* [39] highlights that the stress distribution evaluated at the integration points can present non-negligible oscillations while the same variable evaluated at the nodes is smooth.

Models with and without contact of crack flanks were tested, in order to understand the effect of crack closure. Since the contact of the crack flanks is modelled using a rigid plane in the symmetry plane, the elimination of this contact surface allows the virtual penetration of the crack flanks. Thus, the contact constrains imposed to the nodes of the crack flanks are eliminated to remove crack closure effect. As already mentioned, this numerical strategy is very interesting to quantify the relative importance of PICC and residual stresses on FCG rate.

Table 1
Material parameters used in Swift isotropic hardening law coupled with the Armstrong–Frederick kinematic hardening law.

Material	Y_0 [MPa]	C [MPa]	n	C_X	X_{Sat} [MPa]
Ti-6Al-4V	823.5	707.1	−0.029	104.3	402.0

3. Validation with experimental results

Experimental work was developed for validation of the numerical procedure. CT specimens with the geometry indicated in Fig. 1 and a thickness of 6 mm were tested in a servo-hydraulic testing machine at room temperature. The specimens were manufactured by Lasercusing®, with layers growing towards the direction of loading application. The samples were processed using a ProX DMP 320 high-performance metal additive manufacturing system, incorporating a 500 W fibber laser. After manufacturing by SLM, the specimens were subjected to a stress relieve heat treatment that consisted of a slow and controlled heating up to 670 °C, followed by maintenance at 670 °C ± 15 °C for 5 h in argon medium at atmosphere pressure and finally by cooling to room temperature in air. Fatigue tests were carried out in agreement with the ASTM E647 standard, at room temperature using a 10 kN capacity Instron EletroPuls E10000 machine, under load control.

Fig. 3 compares the numerical predictions with experimental results obtained under constant amplitude loading for stress ratios of 0.05 and 0.4. The slopes of the numerical curves are according the experimental trends. Besides, the increase of stress ratio increases FCG rate in both numerical and experimental tests. The effect of stress ratio is more pronounced in the experimental results, anyway, a reasonable agreement may be found. The reason of the difference observed at R = 0.4 between the numerical predictions and the experimental results is not clear. It may be the presence of other damage mechanisms, apart from cyclic plastic deformation, namely growth and coalescescence of microvoids and environmental damage.

Fig. 4 compares numerical predictions with experimental results, in the presence of a single overload. Note that in the experimental work only one measurement was made in the region affected by the overload, which affects the accuracy of experimental results. In fact, this region is very small, which made it difficult to obtain several measurement points. On the other hand, in the numerical work, the small size of finite elements makes it possible to obtain multiple measurement points and thus well-defined trends. Therefore, the comparison between experimental and numerical results must be done with caution. The only conclusion that can be drawn is that the experimental results do not contradict the numerical trends. In addition, it is recommended to take more detailed measurements in experimental works involving the measurement of FCG rate in the presence of load changes, when the materials have relatively low crack closure levels. In conclusion, although the differences registered in Figs. 3 and 4, the numerical work

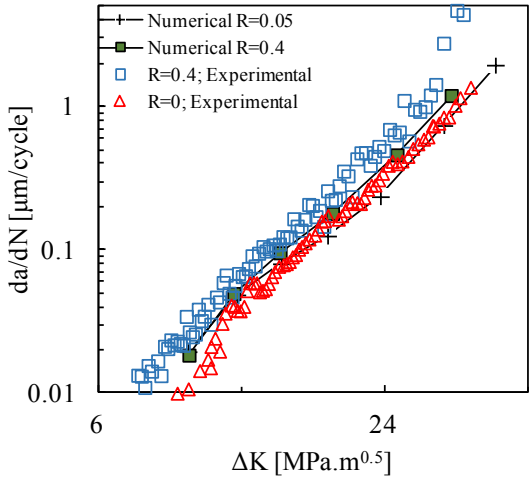

Fig. 3. Comparison between numerical predictions and experimental results under constant amplitude loading (numerical: plane stress, $\Delta\varepsilon^p = 1.533$).

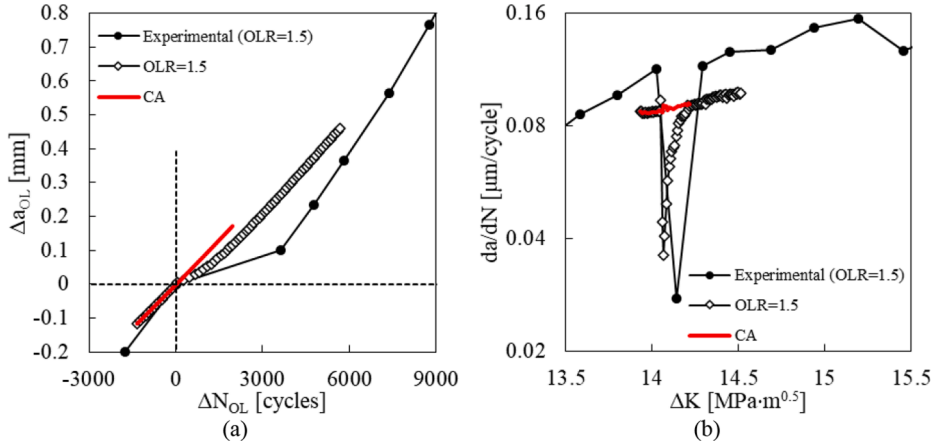

Fig. 4. Comparison between numerical predictions and experimental results in the presence of a single overload. (a_0 = 12.416 mm, a_{OL} = 12.75 mm, R = 0.4, F_{min} = 27.9 N, F_{max} = 69.75 N, F_{OL} = 90.675 N, $\Delta\varepsilon^p$ = 1.533, plane stress).

was able to capture the global trends observed experimentally, therefore is perfectly adequate to develop parametric studies about the effect of different parameters like the overload ratio or crack length.

4. Numerical results

4.1. *da/dN versus Δa*

Fig. 5a illustrates the typical transient crack growth behaviour when a specimen is subjected to a single overload, where a_{OL} and N_{OL} are the crack length and the number of cycles at which the overload is applied, respectively. Generally, the magnitude and extent of retardation is quantified by the parameters defined in Fig. 5a. The number of delay cycles (N_{D1}) is the difference between the number of cycles required to achieve the steady state (N_{D2}) and the number of cycles required for the same crack length at constant amplitude (CA) baseline loading. The overload affected crack growth increment (Δa_{OL}) is the crack growth distance between the point of overload application and the point at which the crack growth rate recovers the baseline value. The crack growth response plotted in function of the crack length from the overload event is illustrated in Fig. 5b, highlighting the crack increment from the overload event corresponding to the minimum crack growth rate reached (Δa_{min}).

Fig. 6a plots the numerical values of *da/dN* versus crack growth, where negative and positive values of ($a - a_{OL}$) represent the crack propagations before and after the overload application, respectively. Considering the loading at constant amplitude, two regimes can be identified. First, there is a decrease of *da/dN* with the propagation of the crack, due to the stabilization of cyclic plastic deformation and formation of residual plastic wake [36]. After this transient regime, there is a slight increase of *da/dN* with crack growth, due to the effect of crack length on crack tip fields. A horizontal dashed line was added to highlight this increase. In the variable amplitude loading, *da/dN* has a sudden increase after the overload application due to the quick development of plastic strain at the crack tip. However, the values of *da/dN* reduced in the next crack increments showing an effect of load history. *da/dN* continues to decrease with crack propagation down to a minimum value, showing delayed retardation. As the crack tip grows inside the plastic zone induced by the overload, *da/dN* gradually increases, tending to the rates found before the overload. In other words, there is a progressive dissipation of the effect of overload. The extent of crack length affected by the overload was about 0.25 mm, which is a relatively small value. The vertical dashed line on the right-hand side indicates the limit of monotonic plastic zone generated by the overload. As can be seen, it seems to exist a good agreement between this plastic zone and extent of crack length affect by the OL.

Fig. 6b plots the crack size as a function of the number of load cycles. In the first load cycles, before the OL, the constant amplitude and overload trends are overlapped as could be expected. After the application of the overload, the rate of increase of *a* is reduced, and after some propagation it returns to the constant amplitude value. The horizontal difference between CA and OL curves is the effect of OL on the number of load cycles required to propagate the crack. These trends are perfectly in accordance with literature [5–7], which is a good indication for the robustness of the numerical approach.

Fig. 7a shows the variation of crack closure phenomenon with crack growth. The level of crack closure was quantified by U^*, which is the percentage of load range during which the crack is closed:

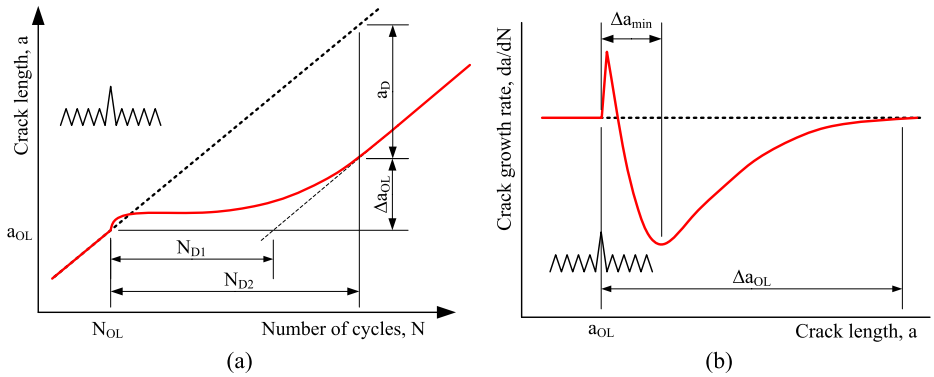

Fig. 5. Effect of a single overload on the fatigue crack growth behaviour: (a) Crack size versus number of load cycles; (b) FCG rate versus crack length.

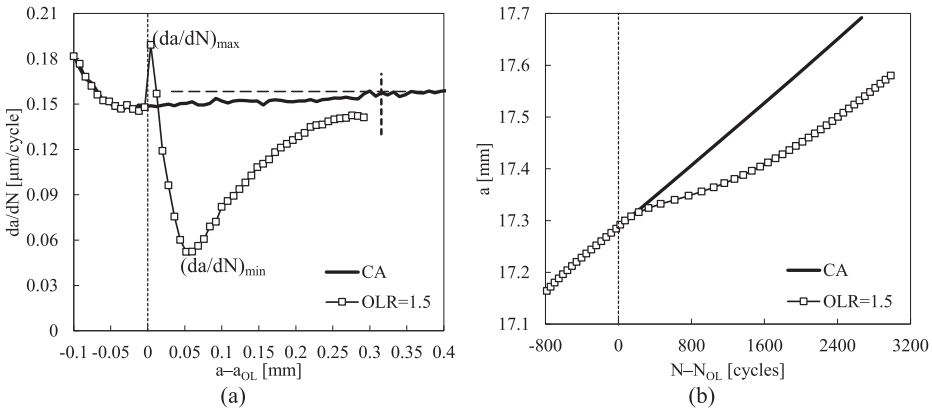

Fig. 6. Effect of an overload on (a) FCG rate versus crack increment. (b) Crack size versus number of load cycles (a_{OL} = 17.4 mm, ΔK_{BL} = 20 MPa·m$^{0.5}$, OLR = 1.5, plane stress).

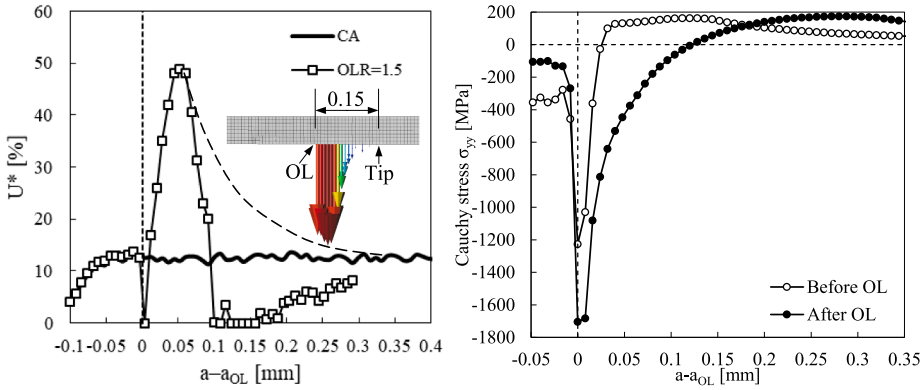

Fig. 7. Effect of an overload on (a) Crack closure level. (b) Predicted stress σ_{yy} ahead of the crack tip before and after a single overload (a_{OL} = 17.4 mm, ΔK_{BL} = 20 MPa·m$^{0.5}$, OLR = 1.5, plane stress).

$$U^* = \frac{F_{open} - F_{min}}{F_{max} - F_{min}} \times 100 \tag{4}$$

where F_{open} is the opening load. In the constant amplitude loading there is an initial increase of U^*, resulting from the formation of residual plastic wake. This increase of U^* explains the decrease of da/dN observed in Fig. 6a. The subsequent stabilized value of U^* is<15%, which is very small for plane stress state. In fact, the Ti-6Al-4V alloy is a high strength material, therefore having relatively small levels of plastic deformation at the crack tip, which reduce crack closure level and also the extent of crack growth affected by the OL. Jesus *et al.* [33] obtained U^*=3.2% using a remote extensometer, and U^*=6.9% using Digital Image Correlation (DIC). The virtual extensometer was placed at a distance of 250 μm behind crack tip and the distance between measurement points was 125 μm. The CT specimen had a thickness of 6 mm, therefore probably is in a stress state between plane stress and plane strain. Considering this thickness and the position of measurement points, lower values of U^* could be expected in the experimental work compared to the numerical predictions. Continuing in Fig. 7a, the overload produces a sudden elimination of crack closure due to crack tip blunting [15]. Subsequently, there is a progressive increase of U^* up to a peak, which seems to be coincident with the minimum of da/dN. Afterwards, there is a progressive decrease down to zero, followed by a progressive increase to the CA value. The second decrease of U^* to zero is unexpected and is not in accordance with da/dN variations. This odd result is explained by partial closure. The crack closure is measured at the first node behind crack tip, but the contact occurs in areas further from the crack tip. The inclusion of this contact in the values of U^* would increase the numerical values to the dashed line. The representation that was superimposed in Fig. 7a shows the contact forces behind crack tip, at minimum load and for $(a - a_{OL}) = 0.15$ mm. The contact of crack flanks occurs at some distance behind crack tip. This phenomenon is naturally included in the numerical model used here, but may be a problem in approaches based on ΔK_{eff}.

Fig. 7b shows the effect of OL on residual stresses measured at minimum load. Under constant amplitude loading, i.e., before OL, there is a small region submitted to residual compressive stresses ahead of crack tip, with a peak value of 1200 MPa at the crack tip. At a distance of 29 μm, there is a transition to tensile stresses. The overload produces a dramatic change of stress distribution. The maximum value of compressive stress increases to 1700 MPa and the region submitted to compressive stresses extended to 120 μm. Therefore, both the residual stresses and crack closure are affected by the OL.

The numerical predictions of da/dN presented in Fig. 6a were obtained dividing the crack increment (8 μm of element size) by the number of load cycles required to reach the critical value of plastic strain. Thus, this FCG rate is an average for each crack increment, i.e. the FCG rate is assumed constant in each crack increment. Therefore, the peak value of da/dN deserves a closer look since it occurs due to a single loading cycle. Fig. 8a shows the accumulation of plastic strain, ε^p, at the crack tip with pseudotime. The sudden drops of ε^p on the left and right sides correspond to the propagation of the crack, i.e., the crack tip advances to the next node, where ε^p is significantly lower. Also, ε^p is not zero at the new crack tip node, because some plastic strain had already been felt at this position. As the load cycles are applied, there is a progressive accumulation of plastic strain. Propagation by node release occurs when the total plastic strain, $\Delta\varepsilon^p$, reaches the critical value defined at the beginning of the simulations, $\Delta\varepsilon^p = 1.533$. In the situation

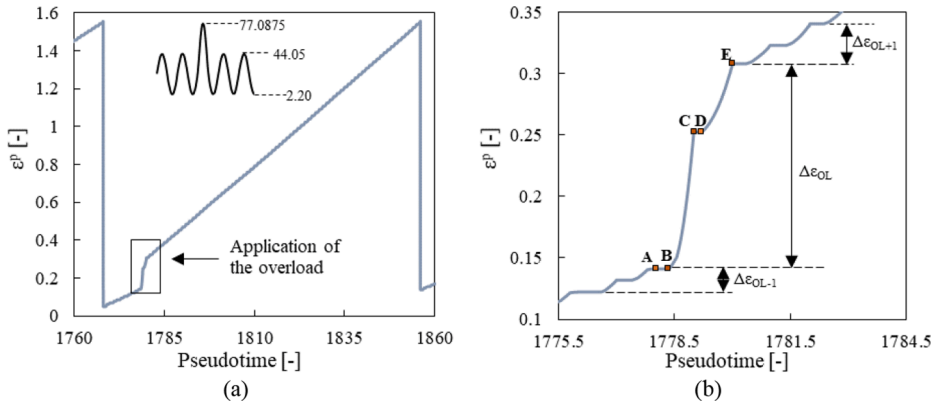

Fig. 8. (a) Crack tip accumulated plastic strain versus load cycles. (b) Detail on the application of an overload (a_{OL} = 16.12 mm, ΔK_{BL} = 18.3 MPa·m$^{0.5}$, OLR = 1.75, plane stress).

illustrated in Fig. 8a, 44 load cycles were made between crack propagations, which results in an average *da/dN* equal to 0.182 μm/cycle. However, the damage accumulation is not uniform with cyclic loading. The overload produces a sudden jump in ε^p, which means that it produces significant damage at the crack tip. Besides, the slope of ε^p versus time curve is higher after the overload than before the overload, which can be attributed to the elimination of crack closure due to crack tip blunting. All these phenomena correspond to a single point in Fig. 6a, which is the peak of *da/dN* at $a - a_{OL} = 0$. Fig. 8b is a zoom of the region where the application of the overload takes place. The load cycle corresponding to the overload are highlighted by points from *A* to *E*. The vertical distance, $\Delta\varepsilon_{OL}$, represents the plastic strain produced by the overload. At point *A* begins the charge of the specimen. From point *A* to point *B* no plastic strain is produced, i.e., there is an elastic regime. At stretch *B-C* a large amount of ε^p is suddenly obtained, which corresponds to the elastic–plastic regime during loading. Point *C* corresponds to the peak load, i.e., $F_C = F_{OL}$. From point *C* to *D*, which corresponds to the elastic unloading, ε^p remains constant. At point D, ε^p increases again due to reversed plastic deformation, however the range of ε^p obtained is lower than at stretch *B-C*.

Since the overload leads to an abrupt increase of the plastic strain at the crack tip (see Fig. 8b), the FCG rate was also evaluated using the plastic deformation at the crack tip. Accordingly, the FCG rate is assessed in each loading cycle, using the increment of plastic strain at the crack tip. Since the adopted fatigue crack growth criterion defines a crack increment of 8 μm (element size) when the plastic strain at the crack tip attains the critical value, the FCG rate is defined by the fraction of the critical plastic strain generated in a single loading cycle. In other words, the crack growth corresponding to the overload, Δa_{OL}, is obtained from:

$$\frac{\Delta\varepsilon^p_{OL}}{\Delta\varepsilon^p} = \frac{\Delta a_{OL}}{8} \tag{5}$$

where $\Delta\varepsilon^p{}_{OL}$ is the plastic deformation produced by the overload and $\Delta\varepsilon^p$ is the total plastic strain. The comparison between both methods of evaluating the FCG rate evolution is presented in Fig. 9a and 9b for plane strain and plane stress states, respectively. The assumption of constant FCG rate in each crack increment is a reasonable approximation, except in the overload cycle. Indeed, in the overload cycle, the FCG rate predicted with the increment of plastic deformation at the crack tip is at least 3 times higher than the one evaluated assuming constant FCG rate within each crack increment, as shown in Fig. 9a. Despite the FCG rate in the overload cycle is identical for plane strain and plane stress conditions, the acceleration of the FCG rate immediately after the overload is negligible when plane strain conditions are adopted (Fig. 9a). The differences observed between plane stress and plane strain states may be explained by crack closure.

The peak of *da/dN* is studied here assuming that crack tip plastic deformation is the crack driving force, however other mechanisms may exist dependent on the maximum load. Wheatley *et al.* [40] studied 316L stainless steel and suggested that the peak of crack growth stems from void and quasi-cleavage fracture within the fatigue damage zone in the vicinity of the crack tip. Li *et al.* [6] studied CT specimens with a thickness of 1.4 mm made of DP780 dual phase steel. They used SEM to conclude that during the application of overload, a damage zone was formed ahead of the crack tip was characterized by cleavage surfaces, tearing ridges, dimples and voids.

The analysis of the crack tip opening displacement, CTOD, usually provides a good understanding of crack tip phenomena. Therefore,

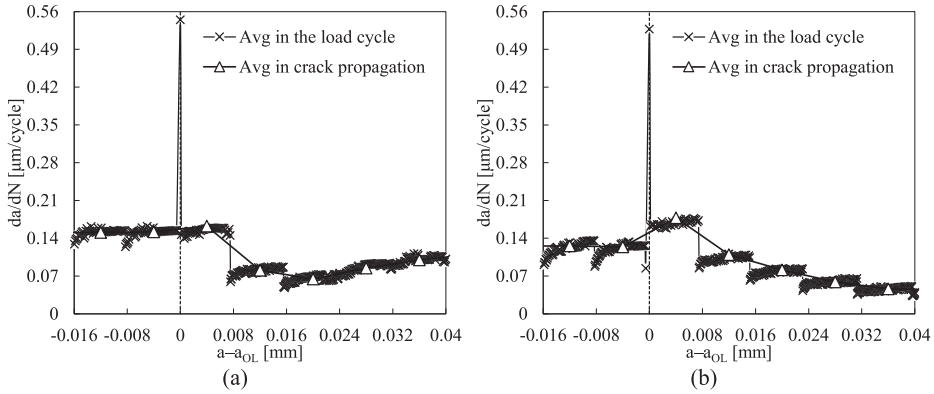

Fig. 9. Comparison of the FCG rate predicted in each loading cycle and predicted in each crack propagation for a single overload at a_{OL} = 16.12 mm of crack length (ΔK_{BL} = 18.3 MPa·m$^{0.5}$) and OLR = 1.5, considering: (a) plane strain conditions; (b) plane stress conditions.

Fig. 10a shows the evolution of CTOD with the application of an overload, for a better understanding of the results presented in Fig. 8b. The CTOD was evaluated at the first node behind the crack tip, therefore at a distance of 8 μm. The baseline loads were F_{min} = 2.20 N and F_{max} = 44.05 N. At region I, despite the increase of F, the crack is closed, being CTOD equal to zero. After that, the crack opens, and first it experiences elastic deformation, characterized by a linear development between CTOD and remote load, F (region II). As F increases in magnitude, the elastic regime is surpassed and plastic blunting begins, as evidenced by the non-linear evolution of CTOD (region II). When the maximum baseline load is exceeded (vertical dashed line), a sudden and pronounced variation of the slope of the CTOD-F curve is observed, as a result of the higher levels of rate of plastic deformation (region III). At this point, the material has not yet been exposed to these stress levels and in response, shows higher plastic deformation levels due to lower material hardening, being the plastic deformation higher with the increase of overload ratio, as expected. Material hardening is therefore of major importance to explain the effect of an overload. During the discharge, plastic blunting is gradually reduced, first linearly, and then non-linearly (region IV). Residual plastic blunting is still obtained at minimum load due to the non-existing closure of the crack, even for the lowest OLR applied. Note that the level of crack closure observed for the baseline loading was relatively small, therefore only a small blunting is required to eliminate it. The level of residual plastic blunting obtained increases with OLR, being of 3.5 μm for OLR = 2.0. The overload loop corresponding to OLR = 1.75 is divided by points from A to E, which correspond to the same points identified in Fig. 8b. At point A begins the charge of the specimen. At point B occurs the transition between the purely elastic and the elastic–plastic regime, which gives rise to an increase of plastic deformation until reaching point C, in accordance with Fig. 8b. During unloading, first the material experiences elastic deformation, stretch C-D, and then an elastic–plastic regime with a progressive increase of plastic deformation. The higher values of plastic strain achieved during the loading of the specimen (see Fig. 8b) are also in accordance with the higher values of CTOD. Also, as illustrated in Fig. 10a, stretch A-B is longer than C-D, which is also in accordance with Fig. 8b, due to crack closure. The link between ε^p, measured at the crack tip, and CTOD, measured behind the tip show the complementarity of these two non-linear parameters.

Fig. 10b plots CTOD versus remote load, F, for three load cycles: the cycle before overload (OL-1), the overload cycle (OL) and the cycle after overload (OL + 1), for a single tensile overload applied at a_{OL} = 16.12 mm, being OLR = 1.75, in plane stress conditions. Crack closure is observed before the application of overload. Higher values of CTOD are achieved in the overload cycle, as already observed in Fig. 10a. When the baseline values of load are surpassed, the rate of CTOD increases, which indicates an easier plastic deformation. As stated in Fig. 10a, the material has not experienced these higher loads and therefore it shows high levels of plastic deformation. After unloading there is no closure of the crack (i.e., CTOD greater than 0 at F_{min}), showing residual plastic blunting. In the case of the cycle immediately after the overload application, there is no crack closure and the levels of plastic deformation are substantially reduced, compared to the overload cycle. The elimination of crack closure explains the higher slope of ε^p-time curve observed after the OL in Fig. 8b.

4.2. Effect of the OLR

The effect of the overload ratio (OLR) on the predicted FCG rate is presented in Fig. 11 for a single overload applied at a_{OL} = 16.12 mm of crack length (ΔK_{BL} = 18.3 MPa·m$^{0.5}$), considering both plane strain and plane stress conditions. Negative values of ($a - a_{OL}$) represent the crack propagation before the overload application, which is required to stabilize the cyclic plastic deformation, particularly under plane stress conditions (see Fig. 11b). The overload was applied only after stabilisation. The same behaviour is observed independently of OLR: a sudden increase followed by a decrease to a minimum value which is reached at some point ahead of the overload application and finally a gradual approximation to the constant amplitude crack growth level. The increase of the overload ratio leads to a decrease of the minimum FCG rate and increase of the OL-affected crack growth increment. Considering plane strain conditions, the minimum value of FCG rate occurs closer to the point of overload application and the gradual convergence to the constant amplitude crack growth level is quicker (compare Fig. 11a and 11b). The effect of OLR predicted numerically is similar to that observed in literature [6,7]. Borrego *et al.* [9] studied MT specimens with a thickness of 3 mm made of 6082-T6 aluminium alloy. The trends obtained experimentally are perfectly similar to the results presented in Fig. 11. However, the region affected by the OL was significantly larger, extending up to 10 mm. In fact, the extent of crack growth affected by the overload greatly depends on material. The titanium alloy studied here is a high strength material, which explains the relatively small extension of the OL affected zone. Bacila *et al.* [41] proposed that lower yield stress produces larger crack length affected by the delay. The increase of yield stress also reduced the crack increment corresponding to the minimum *da/dN*. According them, the higher yield stress induces more intensive residual compressive stresses in a smaller overload plastic zone.

The effect of the overload ratio on crack length evolution is presented in Fig. 12 for a single overload at a_{OL} = 16.12 mm of crack length (ΔK_{BL} = 18.3 MPa·m$^{0.5}$), considering both plane strain and plane stress conditions. For the same value of overload ratio, the number of delay cycles is significantly larger when plane stress conditions are assumed in the numerical simulation. Besides, the increase of the overload ratio leads to

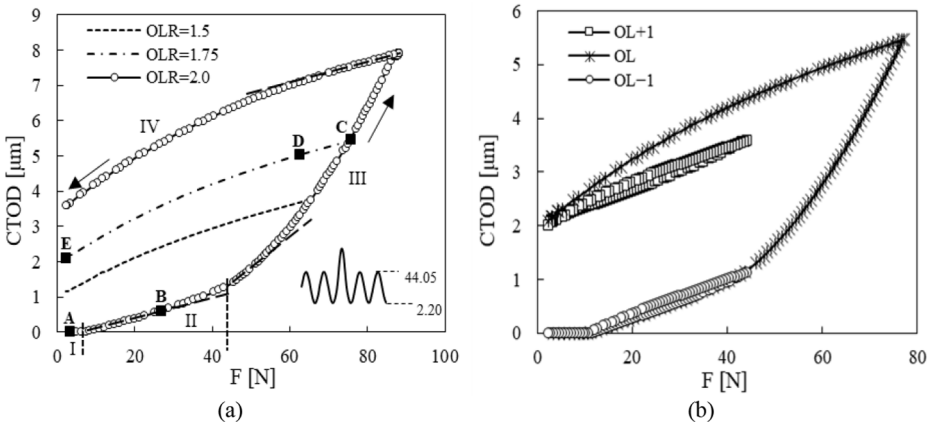

Fig. 10. Evolution of the crack tip opening displacement with applied load for a single overload at a_{OL} = 16.12 mm of crack length (ΔK_{BL} = 18.3 MPa·m$^{0.5}$), under plane stress: (a) Effect of the overload ratio (OLR) on the predicted CTOD; (b) Comparison of CTOD vs F curves obtained before and after the overload for OLR = 1.75.

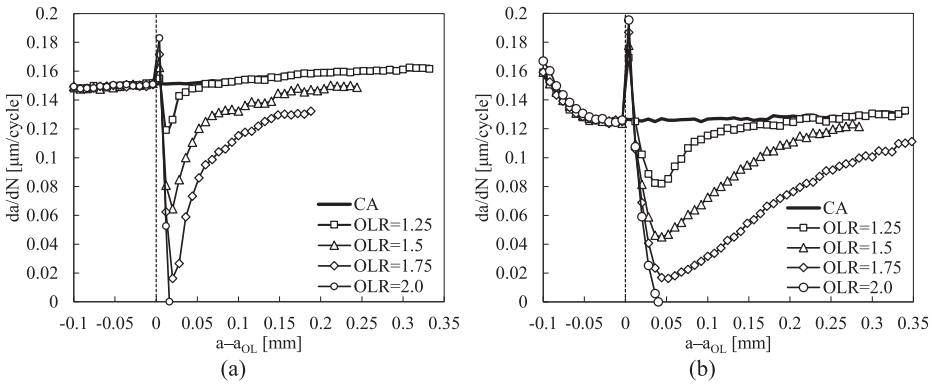

Fig. 11. Effect of the overload ratio (OLR) on the predicted FCG rate for a single overload at $a_{OL} = 16.12$ mm of crack length ($\Delta K_{BL} = 18.3$ MPa·m$^{0.5}$), considering: (a) plane strain conditions; (b) plane stress conditions.

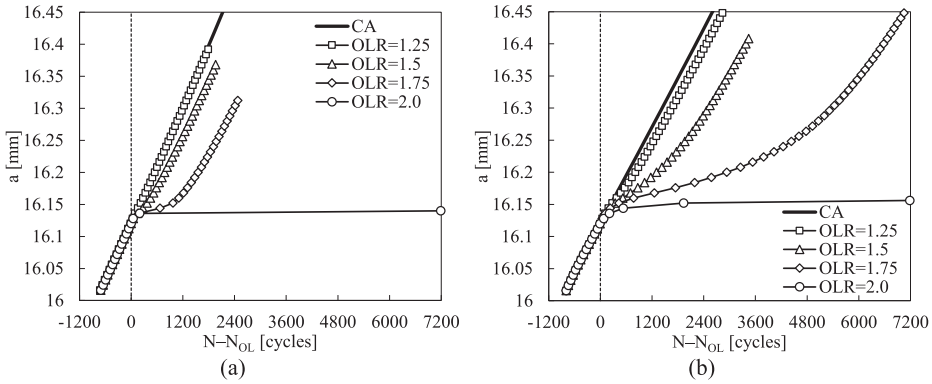

Fig. 12. Effect of the overload ratio (OLR) on the predicted for crack length evolution for a single overload at $a_{OL} = 16.12$ mm of crack length ($\Delta K_{BL} = 18.3$ MPa·m$^{0.5}$), considering: (a) plane strain conditions; (b) plane stress conditions.

an increase of the number of delay cycles. Indeed, crack arrest (i.e., crack stops growing) is observed for OLR = 2.0 since the plastic deformation at the crack tip stopped (see Fig. 11). Non-propagating cracks were experimentally observed after an overload by different authors [42–44]. Bathias and Vancon [45] observed the stop of crack propagation in 2024 and 2618 aluminium alloys for OLR above 2.4. Taheri *et al.* [46] found crack arrest for OLRs greater than 2 or 3. Nelson [47] found that full crack arrest may occur for overload ratios between 2.0 and 2.7. A significant influence of material behaviour on this limit may be expected. If the crack stops due to crack closure, re-start of crack growth can only happen with re-nucleation of FCG [18]. In the numerical simulation, the crack stops when there is no increment of plastic deformation at the crack tip. Crack nucleation, which may occur at a load level that does not produce macroscopic plastic deformation, is not simulated in the present numerical model. In other words, a crack submitted to a relatively large OLR may stop in the numerical simulation, but may re-nucleate in the experimental work. Lu [7] studied experimentally CT specimens with a thickness of 2.5 mm made of QSTE340TM steel. They observed experimentally that the crack with an OLR of 2 and a baseline R = 0.1 and 0.3 needs a large number of load cycles to re-initiate.

The predicted number of delay cycles is presented in Fig. 13 for a single overload applied at $a_{OL} = 16.12$ mm of crack length ($\Delta K_{BL} = 18.3$ MPa·m$^{0.5}$), comparing plane strain and plane stress conditions. Considering the same overload ratio, the number of delay cycles is significantly larger adopting plane stress conditions. Besides, the delay cycles increase with OLR, presenting a relationship approximately exponential, particularly under plane stress conditions. Note that a logarithmic scale is used in the vertical axis. Indeed, the number of delay cycles is an excellent parameter to quantify the effect of overloads or

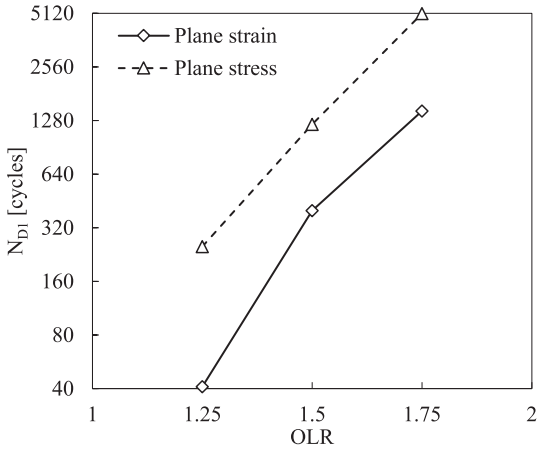

Fig. 13. Effect of the overload ratio (OLR) on predicted delay cycles for a single overload at $a_{OL} = 16.12$ mm of crack length ($\Delta K_{BL} = 18.3$ MPa·m$^{0.5}$).

periodic overloads [48]. In fact, the OL may be intentionally applied to extend fatigue life [9,49,50]. McEvily *et al.* [51] studied the effect of thickness on delay cycles. The increase of the thickness (towards to plane strain) reduced the crack-opening level, increasing FCG rate. As a result, the number of delay cycles decreased with increasing thickness. Ishihara *et al.* [16] studied the effect of stress ratio, R. In tests using CT specimens, N_{D1} increased with R, whereas in tests using center-cracked specimens N_{D1} decreased with R. In both studies, the delay was associated with PICC.

Fig. 14 presents the maximum and minimum values of *da/dN* versus

OLR, considering both plane strain and plane stress conditions. The maximum values of *da/dN* were evaluated using the increment of plastic strain at the crack tip induced by a single loading cycle, as described in the analysis of Fig. 9. The maximum value of *da/dN*, which occurs during the overload, is strongly influenced by the OLR, presenting a progressive increase. The ratio between the maximum *da/dN* and the baseline *da/dN* increases exponentially. Considering plane stress conditions, the maximum *da/dN* is approximately 10 times higher than the baseline *da/dN* for OLR = 2.0. On the other hand, the minimum values of *da/dN* decrease progressively with the OLR, as consequence of the delayed retardation of crack growth. In fact, for OLR = 2.0 the crack stops, i.e. the minimum value of *da/dN* is zero. Nevertheless, considering the extrapolation of the curves without the value corresponding to the OLR = 2.0, the range for which the *da/dN* is zero is 1.85 < OLR < 1.95 and 1.9 < OLR < 2.0 for plane strain and plane stress conditions, respectively. The difference between maximum and minimum values of *da/dN* is larger when plane stress conditions are assumed, in comparison with the plane strain conditions.

4.3. Effect of crack length, a_0

The influence of the baseline-level loading on the predicted FCG rate is presented in Fig. 15 for a single overload of OLR = 1.5, considering both plane strain and plane stress conditions. The increase of the baseline cyclic stress intensity factor (ΔK_{BL}) leads to an increase of the initial acceleration of the FCG rate occurring immediately after an overload. Indeed, for the lower value of ΔK_{BL}, the period of initial acceleration was not detected, particularly in plane strain conditions. The crack growth retardation increases with ΔK_{BL}, i.e., the minimum value of the FCG rate reached during the delayed retardation phase decreases from 0.073 to 0.012 μm/cycle for $\Delta K_{BL} = 14$ MPa·m$^{0.5}$ and from 0.15 to 0.05 μm/cycle for $\Delta K_{BL} = 20$ MPa·m$^{0.5}$ (assuming plane stress conditions). Besides, the distance to the point at which this minimum occurs increases from the lower to the higher ΔK_{BL}. Since the plastic wake increases for larger values of ΔK_{BL}, the increase of the baseline cyclic stress intensity factor leads to an increase of the OL-affected crack growth increment. Jesus *et al.* [33] also observed an increase of the effect of OL with crack length.

Fig. 16 presents the predicted Δa_{min} for a single overload of OLR = 1.5, considering both plane strain and plane stress conditions. The predicted value of Δa_{min} increases linearly with the ΔK_{BL}. This linearity was also experimentally observed by Borrego *et al.* [9] for the 6082-T6 aluminium alloy under different values of stress ratio. Nevertheless, the predicted value is approximately twice in plane stress conditions in comparison with plane strain conditions. Considering plane strain conditions, the crack length Δa_{min} represents <5% of the overload affected crack length, Δa_{OL}, while for plane stress conditions the crack length Δa_{min} represents <10% of Δa_{OL}. This range of values for the crack length Δa_{min} under plane stress conditions is in agreement with the experimental results obtained by Borrego *et al.* [9] for MT specimens with 3 mm of thickness.

5. Discussion

The relative importance of crack closure and residual stresses is a major issue in the analysis of the effect of overloads. In order to understand the effect of crack closure, the contact of crack flanks was removed in the numerical models. This numerical trick has not been exploited by other authors, but is ideal to isolate the effect of PICC. The experimental elimination of crack closure was exploited [52], however it is very difficult to remove material from crack flanks up to the crack tip. The alternative considered experimentally is the increase of baseline stress ratio [18], assuming that this eliminates crack closure. In here, crack closure was eliminated virtually, which can be done for any stress ratio.

Fig. 17a compares FCG rates obtained with and without contact of crack flanks. Without contact, there is no significant effect of overload on FCG. There is only a small peak of *da/dN* when the OL is applied. After that there is a progressive increase of *da/dN* with crack length, which is explained by the effect of crack length on crack tip fields. The results from OLR = 1.25 and 1.5 are overlapped, which indicates that overload ratio does not affect this propagation. The inclusion of crack closure produces a dramatic effect on FCG rate, and the typical variation of *da/dN* associated with an OL is now seen. The difference of FCG observed before the overload is due to the effect of crack closure. Fig. 17b shows the residual stresses ahead of crack tip immediately after the overload for OLR = 1.25, with and without contact of crack flanks. The contact has a minor influence on these results. So, the inclusion of contact of crack flanks in the numerical models produces a major effect on crack closure and *da/dN*, but no effect on residual stresses. Therefore, the variation of *da/dN* after an OL must be associated with the variations of crack closure. Fig. 18 shows similar results, but for a baseline stress ratio R = 0.6. Residual stresses remain unaffected by the contact of crack flanks and crack closure remains responsible for the effect of OL. These results are very relevant in the context of FCG. The only assumption is that cyclic plastic deformation is the main crack driving force, which is widely accepted in the fatigue community.

Note these results clearly contradict the different authors claiming for the relevance of residual stress on post-overload behaviour [7,18–22,53]. The isolation of the effect of crack closure phenomenon by the numerical elimination of the contact of crack flanks has not been reported. This is the only strategy that guarantees the elimination of crack closure.

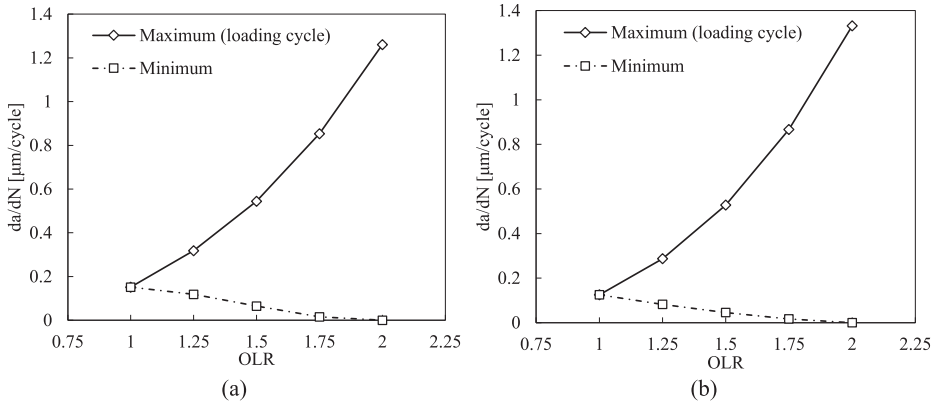

Fig. 14. Effect of the overload ratio (OLR) on the extreme values of predicted FCG rate for a single overload at $a_{OL} = 16.12$ mm of crack length ($\Delta K_{BL} = 18.3$ MPa·m$^{0.5}$) and OLR = 1.5, considering: (a) plane strain conditions; (b) plane stress conditions.

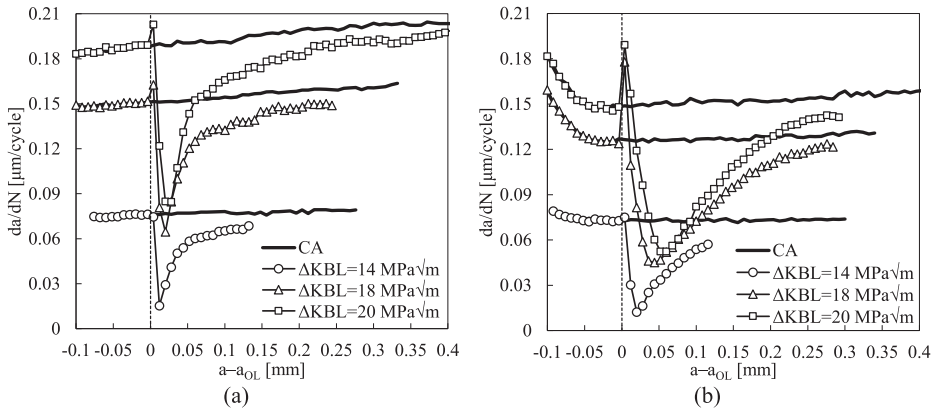

Fig. 15. Effect of the baseline-level loading on the predicted FCG rate for a single overload of OLR = 1.5, considering: (a) plane strain conditions; (b) plane stress conditions.

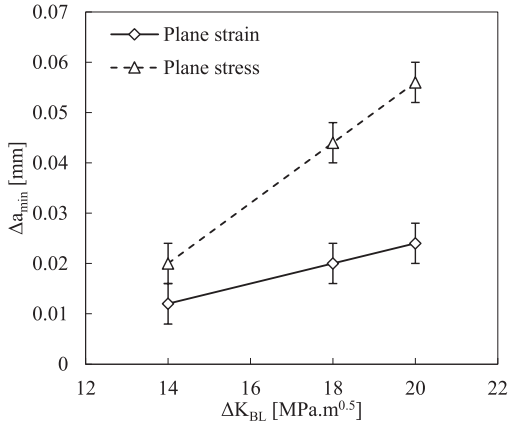

Fig. 16. Effect of the baseline-level loading on the crack length corresponding to maximum retardation for a single overload of OLR = 1.5.

6. Conclusions

Fatigue crack growth (FCG) was predicted numerically in CT specimens made of Ti-6Al-4V and submitted to an overload (OL), assuming that cumulative plastic strain is the crack driving force. The main conclusions are:

- The numerical procedure was found to be very robust, giving the typical variation of *da/dN* after an overload. Besides, the predicted effects of overload ratio, stress state and crack length on *da/dN-a* and *a*-N curves were qualitatively correct.
- The crack length affected by the OL and the crack closure levels were found to be relatively small, which was explained by the high strength of the material.
- A significant effect of stress state was found. Under plane strain conditions, the crack length affected by the overload is smaller and the minimum value of FCG rate occurs closer to the point of overload application than for plane stress conditions. The number of delay cycles is significantly larger for plane stress state.
- Both the residual stresses and crack closure were found to be affected by the OL.
- For an overload ratio of 2.0, the peak value of *da/dN* was found to be approximately 10 times higher than the baseline value.
- In order to understand the effect of crack closure, the contact of crack flanks was removed in the numerical models. Without contact, there is no significant effect of overload on FCG. The inclusion of contact in the numerical models produced a major effect on crack closure and *da/dN*, and no effect on residual stresses. Therefore, the variation of *da/dN* after an OL must be associated with the variations of crack closure.

Author statement

DM Neto wrote the original draft. MF Borges treated the numerical results. FV Antunes made the conceptualization and the final review. J Jesus developed the experimental work.

Funding

This research was funded by projects with reference PTDC/EME-EME/28789/2017 and PTDC/EME-EME/31657/2017, financed by the

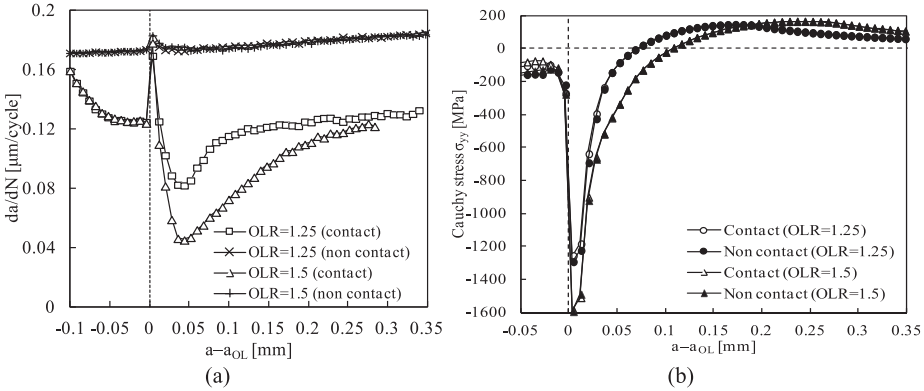

Fig. 17. Effect of the contact between crack flank on the FCG for a single overload at a_{OL} = 16.12 mm of crack length, considering plane stress conditions and a stress ratio R = 0.05. (a) Predicted FCG rate (b) Distribution of the predicted stress σ_{yy} ahead of the crack tip immediately after the overload.

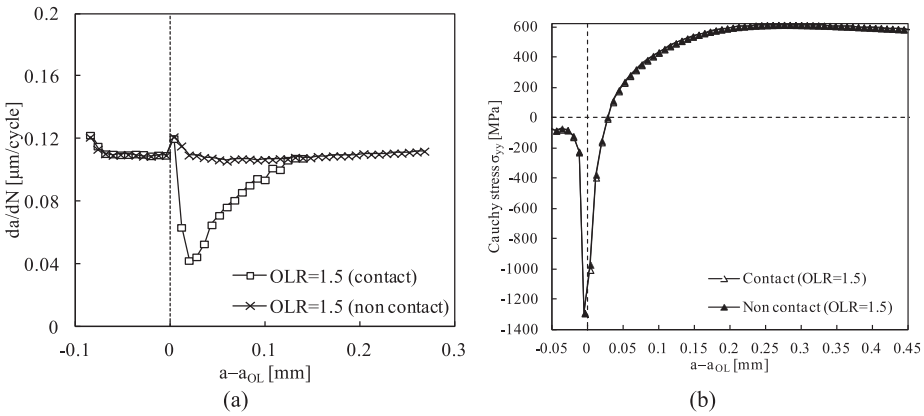

Fig. 18. Effect of the contact between crack flank on the FCG for a single overload at $a_{OL} = 16.12$ mm of crack length, considering plane stress conditions and a stress ratio R = 0.6. (a) Predicted FCG rate. (b) Distribution of the predicted stress σ_{yy} ahead of the crack tip immediately after the overload.

European Regional Development Fund (FEDER), through the Portugal-2020 program (PT2020), under the Regional Operational Program of the Center (CENTRO-01–0145-FEDER-028789 and CENTRO-01–0145-FEDER-031657) and the Foundation for Science and Technology IP/MCTES through national funds (PIDDAC). This research is also sponsored by FEDER funds through the program COMPETE – Programa Operacional Factores de Competitividade – and by national funds through FCT – Fundação para a Ciência e a Tecnologia –, under the project UIDB/00285/2020.

Declaration of Competing Interest

The authors declare that they have no known competing financial interests or personal relationships that could have appeared to influence the work reported in this paper.

References

[1] P. Heuler, H. Klatschke, Generation and use of standardised load spectra and load–time histories, International Journal of Fatigue 27 (8) (2005) 974–990.
[2] J.B. de Jonge, D. Schutz, H. Lowak, J. Schijve, A Standardized Load Sequence for Flight Simulation Tests on Transport Aircraft Wing Structures, NLR TR 73029U, National Aerospace Laboratory (NLR), The Netherlands (1973).
[3] M.A. Wahab, G.R. Rohrsheim, J.H. Park, Experimental study on the influence of overload induced residual stress field on fatigue crack growth in aluminium alloy, J. Mater. Processing Tech. 153-154 (2004) 945–951.
[4] F.J. Pitoniak, A.F. Grandt, L.T. Montulli, P.F. Packman, Fatigue crack retardation and closure in polymethylmethacrylate, Eng. Fract. Mech. 6 (4) (1974) 663–666.
[5] C. Chen, D. Ye, L. Zhang, J. Liu, DIC-based studies of the overloading effects on the fatigue crack pr6opagation behavior of Ti-6Al-4V ELI alloy, International Journal of Fatigue 112 (2018) 153–164.
[6] S. Li, Y. Zhang, L. Qi, Y. Kang, Effect of single tensile overload on fatigue crack growth behavior in DP780 dual phase steel, International Journal of Fatigue 106 (2018) 49–55.
[7] Y.-C. Lu, F.-P. Yang, T.e. Chen, Effect of single overload on fatigue crack growth in QSTE340TM steel and retardation model modification, Engineering Fracture Mechanics 212 (2019) 81–94.
[8] J.M. Vasco-Olmo, F.A. Díaz, M.N. James, B. Yang, Crack tip plastic zone evolution during an overload cycle and the contribution of plasticity-induced shielding to crack growth rate changes, Fatigue Fract Eng Mater Struct 41 (2018) 2172–2186.
[9] L.P. Borrego, J.M. Ferreira, J.M.P. da Cruz, J.M. Costa, Evaluation of overload effects on fatigue crack growth and closure, Eng Fract Mech 70 (2003) 1379–1397.
[10] L. Xiao, D. Ye, C. Chen, J. Liu, L. Zhang, Instrumented indentation measurements of residual stresses around a crack tip under single tensile overloads, Int J Mech Sci 78 (2014) 44–51.
[11] V. Tvergaard, Effect of underloads or overloads in fatigue crack growth by crack-tip blunting, Eng Fract Mech 73 (2006) 869–879.
[12] R.E. Jones, Fatigue crack growth retardation after single-cycle peak overload in Ti–6Al–4V titanium alloy, Eng. Fract. Mech. 5 (3) (1973) 585–604.
[13] A.T. Kermanidis, S.G. Pantelakis, Prediction of crack growth following a single overload in aluminum alloy with sheet and plate microstructure, Eng Fract Mech 78 (11) (2011) 2325–2337.
[14] S. Suresh, Micromechanisms of fatigue crack growth retardation following overloads, Eng. Fract. Mech. 18 (3) (1983) 577–593.
[15] J.B. Baptista, F.V. Antunes, L. Correia, R. Branco, A numerical study of the effect of single overloads on plasticity induced, Theoretical and Applied Fracture Mechanics 88 (2017) 51–63.
[16] S. ISHIHARA, A. MCEVILY, T. GOSHIMA, S. NISHINO, M. SATO, The effect of the R value on the number of delay cycles following an overload, Int. J. Fatigue 30 (10-11) (2008) 1737–1742.
[17] C. SHIN, S. HSU, On the mechanisms and behaviour of overload retardation in AISI 304 stainless steel, Int. J. Fatigue 15 (3) (1993) 181–192.
[18] E. Salvati, H. Zhang, K.S. Fong, X.u. Song, A.M. Korsunsky, Separating plasticity-induced closure and residual stress contributions to fatigue crack retardation following an overload, J. Mech. Phys. Solids 98 (2017) 222–235.
[19] R. Sunder, A. Andronik, A. Biakov, A. Eremin, S. Panin, A. Savkin, Combined action of crack closure and residual stress under periodic overloads: A fractographic analysis, Int Journal of Fatigue 82 (3) (2016) 667–675.
[20] R. Chen, M.-L. Zhua, F.-Z. Xuan, S.-C. Wu, Y.-N. Fu, Near-tip strain evolution and crack closure of growing fatigue crack under a single tensile overload, International Journal of Fatigue 134 (2020), 105478.
[21] C.A. Simpson, S. Kozuki, P. Lopez-Crespo, M. Mostafavi, T. Connolley, P.J. Withers, Quantifying fatigue overload retardation mechanisms by energy dispersive X-ray diffraction , Journal of the Mechanics and Physics of Solids 124 (2019) 392–410.
[22] P. Lopez-Crespo, A. Steuwer, T. Buslaps, Y.H. Tai, A. Lopez-Moreno, J.R. Yates, P. J. Withers, Measuring overload effects during fatigue crack growth in bainitic steel by synchrotron X-ray diffraction, Int J Fatigue 71 (2015) 11–16.
[23] W. He, C. Wang, J. Deng, D. Xie, Z. Zhang, Effect of single tensile overload on fatigue crack growth behavior based on plastically dissipated energy and critical distance theory, Engineering Fracture Mechanics 223 (2020), 106744.
[24] F. Iacoviello, V. Di Cocco, C. Bellini, Overload effects on fatigue cracks in a ferritized ductile cast iron, International Journal of Fatigue 127 (2019) 376–381.
[25] A.A. Aguilar Espinosa, N.A. Fellows, J.F. Durodola, Experimental measurement of crack opening and closure loads for 6082–T6 aluminium subjected to periodic single and block overloads and underloads, Int. J. Fatigue 47 (2013) 71–82.
[26] S. Suresh, Fatigue of materials, Cambridge University Press (1998).
[27] M. MEGGIOLARO, A. MIRANDA, J. CASTRO, L. MARTHA, Crack retardation equations for the propagation of branched fatigue cracks, Int. J. Fatigue 27 (10-12) (2005) 1398–1407.
[28] L. Lawson, E.Y. Chen, M, Meshii, Near-threshold fatigue: a review, Int. J. Fatigue 21 (1999) S15–S34.
[29] L.F. Menezes, C. Teodosiu, Three-dimensional numerical simulation of the deep-drawing process using solid elements, J. Mater. Process. Technol. 97 (2000) 100–106.
[30] ASTM E647 (2016) ASTM E647—standard test method for measurement of fatigue crack growth rates. ASTM B. Stand., 03(July):1–49. www.astm.org.
[31] Thomas J.R. Hughes, Generalization of selective integration procedures to anisotropic and nonlinear media, Int. J. Numer. Meth. Eng. 15 (9) (1980) 1413–1418.
[32] F.V. Antunes, D.M. Rodrigues, Numerical simulation of plasticity induced crack closure: Identification and discussion of parameters, Engng Fracture Mechanics 75 (10) (2008) 3101–3120.
[33] J.S. Jesus, L.P. Borrego, J.A.M. Ferreira, J.D. Costa, C. Capela, Fatigue crack growth behaviour in Ti6Al4V alloy specimens produced by selective laser melting, International Journal of Fracture 223 (1-2) (2020) 123–133.
[34] P. Alart, A. Curnier, A mixed formulation for frictional contact problems prone to Newton like solution methods, Comput. Methods Appl. Mech. Eng. 92 (3) (1991) 353–375.
[35] C.O. Frederick, P.J. Armstrong, A mathematical representation of the multiaxial Bauschinger effect, Mater. High. Temp. 24 (1) (2007) 1–26.
[36] F.F. Ferreira, D.M. Neto, J.S. Jesus, P.A. Prates, F.V. Antunes, Numerical Prediction of the Fatigue Crack Growth Rate in SLM Ti-6Al-4V Based on Crack Tip Plastic Strain, Metals 10 (2020) 1133.
[37] K. Solanki, S.R. Daniewicz, J.C. Newman Jr, Finite element modelling of plasticity-induced crack closure with emphasis on geometry and mesh refinement effects, Engng Fract Mech 70 (2003) 1475–1489.

[38] M.F. Borges, D.M. Neto, F.V. Antunes, Numerical simulation of fatigue crack growth based on accumulated plastic strain, Theoretical and Applied Fracture Mechanics 108 (2020), 102676.
[39] J.P. Brito, M.C. Oliveira, D.M. Neto, J.L. Alves, L.F. Menezes, Influence of the characteristics of the 3D FE mesh on the evolution of variables used to characterize the stress state, AIP Conference Proceedings 2113 (2019), 160015.
[40] G. Wheatley, Y. String, X.Z. Hu, Y. Brechet, Effects of single tensile overload on fatigue crack growth in a 316L steel, J. Fatigue Fracture Eng. Mater. Struct. 22 (1999) 1041–1051.
[41] A. Bacila, X. Decoopman, G. Mesmacque, M. Voda, V. Serban, Study of underload effects on the delay induced by an overload in fatigue crack propagation, International Journal of Fatigue 29 (9-11) (2007) 1781–1787.
[42] P.J. Bernard, T.C. Lindley, C.E. Richards, The effect of single overloads on fatigue crack propagation in steels, Metal Science 11 (8-9) (1977) 390–398.
[43] J.D. Bertel, A. Clerivet, C. Bathias, On the relation between the threshold and the effective stress intensity range during complex loading, ASTM STP 791 (1983) 366–379.
[44] C.S. Shin, N.A. Fleck, Overload retardation in a structural steel, Fatigue Fract. Eng. Mater. Struct. 9 (5) (1987) 379–393.
[45] C. Bathias, M. Vancon, Mechanisms of overload effect on fatigue crack propagation in aluminium alloys, Eng. Fract. Mech. 10 (2) (1978) 409–424.
[46] F. Taheri, D. Trask, N. Pegg, Experimental and analytical investigation of fatigue characteristics of 350WT steel under constant and variable amplitude loading, Mar. Struct. 16 (2003) 69–91.
[47] D.V. Nelson, Review of fatigue crack-growth prediction under irregular loading, Spring Meet, Society for Experimental Stress Analysis, Chicago, IL, 1975, pp. 11–16.
[48] S. Sarkheil, M.S. Foumani, Numerical and experimental study on the optimization of overload parameters for the increase of fatigue life, Aerospace Science and Technology 35 (2014) 80–86.
[49] Raghuvir Kumar, Effect of variable single cycle peak overload on fatigue life, Int. J. Press. Vessels Piping 48 (3) (1991) 293–303.
[50] Öktem Vardar, Effect of single overload in FCP, Eng. Fract. Mech. 30 (3) (1988) 329–335.
[51] A.J. McEvily, S. Ishihara, Y. Mutoh, On the number of overload-induced delay cycles as a function of thickness, International Journal of Fatigue 26 (2004) 1311–1319.
[52] Kokleang Vor, Catherine Gardin, Christine Sarrazin-Baudoux, Jean Petit, Wake length and loading history effects on crack closure of through-thickness long and short cracks in 304L: Part I – Experiments, Engineering Fracture Mechanics 99 (2013) 266–277.
[53] K. Sadananda, A.K. Vasudevan, R.L. Holtz, E.U. Lee, Analysis of overload effects and related phenomena, International Journal of Fatigue 21 (1999) S233–S246.